

Markov random field regularisation models for adaptive binarisation of nonuniform images

D. Shen
H.H.S. Ip

Indexing terms: Adaptive image binarisation, Edge-preserving smoothing, Markov random field models, Standard regularisation, Threshold surface

Abstract: Two related MRF models, an edge-preserving smoothing model followed by a modified standard regularisation, are presented for the adaptive binarisation of nonuniform images in the presence of noise. In particular, a computational model is developed for a modified standard regularisation method which calculates the adaptive threshold surface for noisy images. Since the modified standard regularisation depends only on the image data, and not its edge segments, it gives much better performance and can be applied to more classes of image than those methods that solely rely on edge segments. Experimental results demonstrate that the proposed method has the best performance over three other commonly used adaptive segmentation methods and is faster than previous interpolation-based thresholding techniques.

1 Introduction

Since the Markov random field (MRF) can be used for the reconstruction of a function starting from a set of noisy sparse data, it has been applied widely in the past few years in image reconstruction and segmentation [1–3]. The MRF model is appealing because it describes a system by means of local interactions and is able to capture many interesting features by simply adding appropriate terms in the cost functional. More importantly, there exist many fast algorithms for surface interpolation using wavelet transform [4], hierarchical basis functions [5] and deterministic approximations [6]. Smoothness is one of the most common assumptions in designing MRF models. However, since most image functions contain intensity discontinuities at the edges of objects and have discontinuities in the first derivative at the corners of objects, the image surface reconstructed by the smoothness-based MRF model will be oversmoothed at the locations of such discontinuities. To overcome this, various techniques [7–9] have been proposed to modify the smoothness-based

MRF models to preserve discontinuities. A systematic study of these techniques was provided in [10]. In this work, we first apply an edge-preserving smoothing MRF model for removing noise from the noisy nonuniform data (1-D and 2-D), and then apply another MRF model named the modified standard regularisation to calculate an adaptive threshold surface for the adaptive binarisation of the nonuniformly illuminated data (1-D and 2-D). The reason why the modified standard regularisation is suitable for calculating the adaptive threshold surface is also presented.

In image binarisation, threshold selection method [11] is one of the most popular approaches. An image histogram, or its transformation, is often used as a tool for selecting appropriate threshold. In general, the various histogram transformation method can be unified by using a gray level against edge value scatter plot [12]. However, for noisy and nonuniformly illuminated images, a single fixed threshold, no matter how well chosen, cannot satisfy the requirement of good binarisation. Attempting to overcome this problem, [13, 14] suggest using local distribution information of the image gray-levels to create an adaptive threshold surface. However, these techniques usually fail to give proper binarisation once the created threshold surface is not in coherence with the image content. Accordingly, Yanowitz and Bruckstein [15] proposed a method to interpolate the threshold surface by using the gradient magnitude image. Since they used SORM (successive overrelaxation method) to calculate the threshold surface, the processing time was very long and the resulting threshold surface is usually a local minimal solution of the cost function. We have previously formulated the construction of the threshold surface as an active surface optimisation problem, and solved by Hopfield neural network [16]. With our four proposed constraints which ensure the active threshold surface to conform with the underlying image topography, this method [16] gives faster processing time and superior binarisation particularly for edge segments that are sparsely distributed in the image space.

The two methods in [15, 16] are based on the edge segments of an image, and therefore edge detection is a prerequisite of these two methods. More importantly, the effectiveness of these methods depends on how well the edge segments are detected. In practice, some edge segments may be corrupted by noise or may be lost owing to low contrast, which make the binarisation result unsatisfactory. We propose a substantially more efficient method, which removes the prerequisite process of edge detection, for segmenting noisy and nonuni-

© IEE, 1998

IEE Proceedings online no. 19982314

Paper first received 7th January and in revised form 25th March 1998

The authors are with the Image Computing Group, Department of Computer Science, City University of Hong Kong, Tat Chee Avenue, Kowloon, Hong Kong

form images. This formulation not only saves the processing time but also provides good binarisation results. More specifically, our technique can also be implemented by Hopfield neural network, as in [16].

There exist many locally adaptive threshold methods, and the eleven most promising locally adaptive threshold methods were evaluated by Trier and Jain [17]. The evaluation results are as follows. Niblack's method gave the best performance when using the postprocessing step, while Yanowitz and Bruckstein's method gave the best performance when removing the postprocessing step. As to processing speed, Niblack's method was one of two fastest methods, while Yanowitz and Bruckstein's method was the slowest. Since the speed of Parker's method (one of the these 11 locally adaptive threshold methods evaluated) is between Yanowitz and Bruckstein's method and Niblack's method, it is used here as one of the methods for comparing its binarisation results with our MRF-based method.

In this way we have four binarisation techniques, namely our method, Yanowitz and Bruckstein's method (SORM), Niblack's method, and Parker's method. The binarisation results of the four methods applied to several typical artificial/real images are compared in this paper, and our method gives the best performance for all the cases. As to processing speed, our method is about seven times faster than Yanowitz and Bruckstein's method. The reasons for our method being faster than SORM are: intensity information on every pixels of image space is used as guiding information in our method, and the smoothness term in the energy functional of our modified standard regularisation has been reformulated.

2 MRF models for image smoothing

MRF models can be used to reconstruct a desired function from a set of noisy data. The reconstruction problems in early vision tend to be mathematically ill-posed since the existence, uniqueness and the stability of solutions cannot be guaranteed in the absence of the supplementary constraints. Various constraints have been suggested, and the smoothness constraint is one of the most common assumptions in MRF models. With additional supplementary constraints, the reconstruction problems may be formulated to become well-posed mathematical forms whose solutions are computable. Additionally, since the general smoothness constraint will lead to undesirable and oversmoothed solutions, studies on edge-preserving smoothing model become important.

In the following Sections, we first give the general mathematical form for the MRF-based image smoothing, then the discrete standard regularisation and finally the edge-preserving smoothing model in the discrete case.

2.1 General MRF models for image smoothing

The energy function of MRF model is the sum of two functionals: the likelihood functional and the smoothness functional. The mathematical expression for the 1-D case is as follows:

$$E(V) = \int_a^b w^L(x)(V(x) - d(x))^2 dx$$

$$+ \sum_{m=1}^M \int_a^b w_m^S(x) g_m(V^{(m)}(x)) dx$$

where V is the reconstructed function from the noisy data d , and a and b are the bounds of the noisy data. The first term represents constraint on the likelihood between the reconstructed function V and the noisy data d , while the second term represents the smoothness constraint imposed on the reconstructed function V . $w^L(x)$ and $w_m^S(x)$ are the prespecified, nonnegative and continuous weighting functions, respectively, for the likelihood functional and the smoothness functional. $g_m(V^{(m)}(x))$ is the potential function, which defines the penalty against the irregularity in $V^{(m-1)}(x)$. When the energy function $E(V)$ is small, the reconstructed function V is a good compromise between smoothness in the sense of minimal stabilising likelihood functional and adhesion to the data in the sense of the minimal sum of squared deviations. Different definitions of g_m therefore lead to different MRF models [10]. Here, we pay special attention to two definitions of g_m , which leads to the two MRF models adopted in this work for adaptive binarisation of non-uniform data.

One definition for the potential function g_m takes the pure quadratic form $g_{sqr}(\xi)$

$$g_m(\xi) = g_{sqr}(\xi) = \xi^2, \quad \text{for } m = 1, 2, \dots, M$$

which is usually called the 'standard regularisation' [18]. Notice that the standard regularisation will result in oversmoothness over the image discontinuities. To date, there exist many potential functions which are both convex and edge-preserving [10, 19], and seven functions were listed in [19]. Among these seven the Huber function, used for computing optical flow involving discontinuities, is shown to be the most suitable one in terms of edge-preserving quality and computational cost [19]. Accordingly, the Huber function $g_{Huber}(\xi)$ is adopted as another definition of g_m :

$$g_m(\xi) = g_{Huber}(\xi) = \begin{cases} \xi^2, & |\xi| \leq \gamma \\ 2\gamma|\xi| - \gamma^2, & |\xi| > \gamma \end{cases}, \quad \text{for } m = 1, 2, \dots, M$$

Similarly, for the 2-D case, the energy function of MRF model can be written as

$$E(V) = \iint_D \left[w^L(x, y)(V(x, y) - d(x, y))^2 + \sum_{m=1}^M w_m^S(x, y) \binom{M}{m} g_m \left(\frac{\partial^M V}{\partial x^m \partial y^{M-m}} \right) \right] dx dy$$

where D is the image space.

2.2 Discrete standard regularisation

The discrete form of the energy functional of the standard regularisation can be obtained from its continuous form shown in the previous Section:

$$E(V) = \sum_{i=1}^{N_x} (V_i - d_i)^2 + \lambda_1 \sum_{i=1}^{N_x} (V'(x_i))^2$$

where $V_i = V(x_i)$, $d_i = d(x_i)$ and x_i represents the i th discrete point. As to the two ending points, $x_1 = a$ and

$x_{N_x} = b$. For clarity and without loss of generality, we assume that $x_i - x_{i-1} = 1$ for $i = 1, 2, \dots, N_x$ after the rescaling process. The total number of the discrete points is N_x , w^L has been set to 1 and w_m^S set to λ_1 . Also, M is set to 1, which means only first-order derivative is considered. Usually, for the i th point ($i > 1$), we can write its first-order derivative $V'(x_i)$ as $V'(x_i) = V_i - V_{i-1}$. Using these definitions and rearranging the energy functional, the energy functional of the standard regularisation can be rewritten in the following form:

$$E(V) = \sum_{i=1}^{N_x} (V_i - d_i)^2 + \lambda_1 \sum_{i=1}^{N_x} V_i \left(\sum_{k=-1}^1 S_1(k+1) V_{i+k} \right)$$

where $S_1 = [-1 \ 2 \ -1]$. Notice that the operators for the boundary points i ($i = 1$ and $i = N$) are different from the operators for the interior points i ($1 < i < N_x$). For simplification, we don't consider these differences in the rearranged equation.

For the 2-D cases, the corresponding energy functional can be similarly defined as

$$E(V) = \sum_{i=1}^{N_x} \sum_{j=1}^{N_y} (V_{i,j} - d_{i,j})^2 + \lambda_1 \sum_{i=1}^{N_x} \sum_{j=1}^{N_y} \left((V_x(x_i, y_j))^2 + (V_y(x_i, y_j))^2 \right)$$

The meanings of the parameters in this equation are similar to those in the 1-D case. Using the similar definitions of the first-order partial derivatives $V_x(x_i, y_j) = V_{i+1,j} - V_{i,j}$ and $V_y(x_i, y_j) = V_{i,j+1} - V_{i,j}$, the energy functional of the 2-D case changes to be

$$E(V) = \sum_{i=1}^{N_x} \sum_{j=1}^{N_y} (V_{i,j} - d_{i,j})^2 + \lambda_1 \sum_{i=1}^{N_x} \sum_{j=1}^{N_y} \left(V_{i,j} \sum_{k=-1}^1 \sum_{l=-1}^1 S_2(k+1, l+1) V_{i+k, j+l} \right)$$

where

$$S_2 = \begin{bmatrix} 0 & -1 & 0 \\ -1 & 4 & -1 \\ 0 & -1 & 0 \end{bmatrix}$$

is a matrix used as an operator.

2.3 Discrete edge-preserving smoothing model

The energy functional for the 1-D discrete edge-preserving smoothing model is

$$E(V) = \sum_{i=1}^{N_x} (V_i - d_i)^2 + \lambda \sum_{i=1}^{N_x} g_{Huber}(V'(x_i))$$

and the energy functional for the 2-D case is

$$E(V) = \sum_{i=1}^{N_x} \sum_{j=1}^{N_y} (V_{i,j} - d_{i,j})^2 + \lambda \sum_{i=1}^{N_x} \sum_{j=1}^{N_y} (g_{Huber}(V_x(x_i, y_j)) + g_{Huber}(V_y(x_i, y_j)))$$

Meanings for parameters in these two equations are similar to those in the discrete standard regularisation, except that the neighbouring penalty terms cannot be combined together to become an integrated description since the potential function $g_{Huber}(\xi)$ in this case is too complicated.

3 Adaptive image segmentation method

In this Section we give the detailed procedures of our method for adaptive binarisation of nonuniform images. We first show why the modified standard regularisation can be used to calculate the adaptive threshold surface. Then we give the energy functional of the modified standard regularisation for obtaining the adaptive threshold surface, and its updating equations are also given. The modified standard regularisation is reformulated and generalised from the standard regularisation, however, as to the speed of constructing the threshold surface, the performance of the modified standard regularisation is much better than that of the standard regularisation. Finally, we show why we must use the edge-keeping smoothing model to smooth the input noisy image before using the modified standard regularisation to calculate the adaptive threshold surface.

In summary, our method for image segmentation can be described as follows:

- smooth the input noisy data by the edge-preserving smoothing model and obtain the smoothed data
- use the modified standard regularisation to calculate the threshold surface based on the smoothed data
- use the threshold surface to segment the smoothed data. Here, the smoothed data is regarded as the object to be segmented.

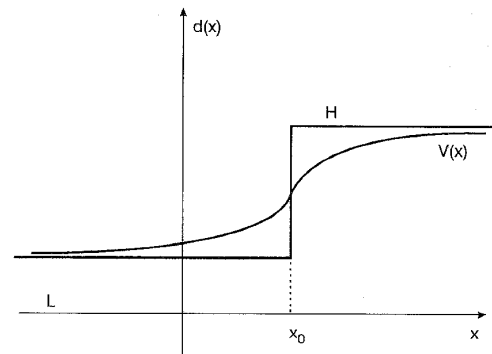


Fig. 1 Ideal step function

3.1 Adaptive threshold surface

3.1.1 Property of standard regularisation

This Section shows, for the 1-D case, the determination of the adaptive threshold surface using standard regularisation. A similar proof can be obtained for the modified standard regularisation, proposed in Section 3.1.2. Assume that data d is the ideal step function, shown in Fig. 1, and $V(x)$ is the adaptive threshold surface calculated from data d by using the standard regularisation. For data d , $d(x) = L$ when $x < x_0^-$ and $d(x) = H$ when $x > x_0^+$. We show in the following that the calculated function $V(x)$ satisfies the following requirements:

$$\begin{cases} V(x) > d(x), & x < x_0^- \\ V(x) < d(x), & x > x_0^+ \end{cases}$$

which means, using $V(x)$ as the threshold surface to segment the data d , we obtain the correct result, i.e. $x < x_0^-$ is background area and $x > x_0^+$ is the object area. The energy functional of the standard regularisation, corresponding to the ideal step function, is

$$E(V) = \int_{-\infty}^{\infty} (V(x) - d(x))^2 dx + \lambda_1 \int_{-\infty}^{\infty} g_{sqrr}(V'(x)) dx$$

Solutions V^* minimising $E(V)$ must satisfy the following Euler equation:

$$2[V(x) - d(x)] - \lambda_1 \frac{d}{dx} [g'_{sqrr}(V'(x))] = 0$$

for $x < x_0^-$ and $x > x_0^+$

Using $g_{sqrr}(\xi) = \xi^2$ the equation becomes $V(x) - d(x) - \lambda V''(x) = 0$, for $x < x_0^-$ and $x > x_0^+$. The solutions for this differential equation is followed and we discuss the solutions respectively in the two domains: $x > x_0^+$ and $x < x_0^-$.

Solution on $x > x_0^+$:

$$V(x) = A_1 e^{\frac{1}{\sqrt{\lambda}}x} + A_2 e^{-\frac{1}{\sqrt{\lambda}}x} + H$$

Notice that the term $A_1 \exp(x/\sqrt{\lambda})$ will become infinite when x becomes infinite. Considering the real situation, it is unreasonable for $V(x)$, as a solution to $E(V)$, to be infinite. Thus the term $A_1 \exp(x/\sqrt{\lambda})$ should be removed from the solution $V(x)$, which leads to

$$V(x) = A_2 e^{-\frac{1}{\sqrt{\lambda}}x} + H$$

Solution on $x < x_0^-$:

$$V(x) = B_1 e^{\frac{1}{\sqrt{\lambda}}x} + B_2 e^{-\frac{1}{\sqrt{\lambda}}x} + L$$

The term $B_2 \exp(-x/\sqrt{\lambda})$ will become infinite when x becomes negative infinite, which is unreasonable in practice and should be removed from the solution $V(x)$. Then

$$V(x) = B_1 e^{\frac{1}{\sqrt{\lambda}}x} + L$$

The solution to $V(x)$ is obtained from two domains $x > x_0^+$ and $x < x_0^-$; it should be continuous at position x_0 . We require that both $V(x)$ and its first derivative $V'(x)$ are continuous at x_0 , and thus obtain the following two constraints:

$$V(x) \text{ continuous: } A_2 e^{-\frac{1}{\sqrt{\lambda}}x_0} + H = B_1 e^{\frac{1}{\sqrt{\lambda}}x_0} + L$$

$$V'(x) \text{ continuous: } -\frac{1}{\sqrt{\lambda}} A_2 e^{-\frac{1}{\sqrt{\lambda}}x_0} = \frac{1}{\sqrt{\lambda}} B_1 e^{\frac{1}{\sqrt{\lambda}}x_0}$$

From the two constraints we then evaluate the constants as

$$A_2 = -\frac{H-L}{2} e^{\frac{1}{\sqrt{\lambda}}x_0}$$

$$B_1 = \frac{H-L}{2} e^{-\frac{1}{\sqrt{\lambda}}x_0}$$

The complete solution to $V(x)$ is

$$V(x) = \begin{cases} H - \frac{H-L}{2} e^{-\frac{1}{\sqrt{\lambda}}(x-x_0)}, & x > x_0^+ \\ L + \frac{H-L}{2} e^{\frac{1}{\sqrt{\lambda}}(x-x_0)}, & x < x_0^- \end{cases}$$

We see that $V(x) > d(x)$ when $x < x_0^-$ and $V(x) < d(x)$ when $x > x_0^+$ and conclude that $V(x)$ can be used as a threshold surface for segmenting the ideal step func-

tion. In fact, the standard regularisation can also be used to construct the threshold surface for segmenting general functions (even when they are nonuniform), since a general function can be approximated by a series of ideal step functions. One can appreciate this observation from the experiments presented in Section 4.

3.1.2 Energy functional of modified standard regularisation: We derive the energy function of the modified standard regularisation by generalising and reformulating the standard regularisation. The energy function of the 1-D standard regularisation is

$$E(V) = \sum_{i=1}^{N_x} (V_i - d_i)^2 + \lambda_1 \sum_{i=1}^{N_x} (-V_{i-1} + 2V_i - V_{i+1}) V_i$$

The energy minimisation approach is usually used to calculate the local minimum of the energy function. Using the energy minimisation approach such as the gradient descent method, we obtain the following updating rule for V_i from time t to time $t+1$:

$$V_i^{(t+1)} = V_i^{(t)} - 2\mu \left[(V_i^{(t)} - d_i) + \lambda_1 (-V_{i-1}^{(t)} + 2V_i^{(t)} - V_{i+1}^{(t)}) \right]$$

for $i = 1, 2, \dots, N_x$

where μ is a learning ratio. With the initial $V_i^{(0)}$, the solution for V_i is $V_i^{(\infty)}$. In the updating equation, the updating information comes from two aspects: the data force ($V_i^{(t)} - d_i$) and the smoothing force ($-V_{i-1}^{(t)} + 2V_i^{(t)} - V_{i+1}^{(t)}$). The objective of the updating equation is to make the solution close to the data and at the same time conform to the smoothness constraint as much as possible. Thus the objective of the standard regularisation can be reformulated as

$$\min_V E(V) = \sum_{i=1}^{N_x} (V_i - d_i)^2$$

$$\text{subject to } Lap_1(i) = (-V_{i-1} + 2V_i - V_{i+1}) = 0, \quad i = 1, 2, \dots, N_x$$

$Lap_1(i)$ is the laplacian operator on V_i . This description means that we can add other penalty terms ($Lap_1(i)$)^p for $p > 2$ into the energy function of the standard regularisation. Here, only the penalty term ($Lap_1(i)$)² is added and then the energy function of the modified standard regularisation is

$$E(V) = \sum_{i=1}^{N_x} (V_i - d_i)^2 + \lambda_1 \sum_{i=1}^{N_x} Lap_1(i) V_i + \lambda_2 \sum_{i=1}^{N_x} (Lap_1(i))^2$$

Rearranging the third term, the equation becomes

$$E(V) = \sum_{i=1}^{N_x} (V_i - d_i)^2 + \lambda_1 \sum_{i=1}^{N_x} V_i \left(\sum_{k=-1}^1 S_1(k+1) V_{i+k} \right) + \lambda_2 \sum_{i=1}^{N_x} V_i \left(\sum_{k=-2}^2 T_1(k+2) V_{i+k} \right)$$

where $T_1 = [1 \ -4 \ 6 \ -4 \ 1]$. Correspondingly, the updating equation of the modified standard regularisation for the 1-D case becomes

$$V_i^{(t+1)} = V_i^{(t)} - 2\mu \left[(V_i^{(t)} - d_i) + \lambda_1 \sum_{k=-1}^1 S_1(k+1)V_{i+k}^{(t)} + \lambda_2 \sum_{k=-2}^2 T_1(k+2)V_{i+k}^{(t)} \right]$$

for $i = 1, 2, \dots, N_x$

Similarly, the energy function of the 2-D standard regularisation can be reformulated as

$$\min_V E(V) = \sum_{i=1}^{N_x} \sum_{j=1}^{N_y} (V_{i,j} - d_{i,j})^2$$

subject to

$$Lap_2(i, j) = \sum_{k=-1}^1 \sum_{l=-1}^1 S_2(k+1, l+1)V_{i+k, j+l} = 0$$

which leads to the energy function of our 2-D modified standard regularisation

$$E(V) = \sum_{i=1}^{N_x} \sum_{j=1}^{N_y} (V_{i,j} - d_{i,j})^2 + \lambda_1 \sum_{i=1}^{N_x} \sum_{j=1}^{N_y} Lap_2(i, j)V_{i,j} + \lambda_2 \sum_{i=1}^{N_x} \sum_{j=1}^{N_y} (Lap_2(i, j))^2$$

Rearranging the third term by using the technique proposed in [16] we obtain the reformulated equation as follows:

$$E(V) = \sum_{i=1}^{N_x} \sum_{j=1}^{N_y} (V_{i,j} - d_{i,j})^2 + \lambda_1 \sum_{i=1}^{N_x} \sum_{j=1}^{N_y} \left(V_{i,j} \sum_{k=-1}^1 \sum_{l=-1}^1 S_2(k+1, l+1)V_{i+k, j+l} \right) + \lambda_2 \sum_{i=1}^{N_x} \sum_{j=1}^{N_y} \left(V_{i,j} \sum_{k=-2}^2 \sum_{l=-2}^2 T_2(k+2, l+2)V_{i+k, j+l} \right)$$

where

$$T_2 = \begin{bmatrix} 0 & 0 & 1 & 0 & 0 \\ 0 & 2 & -8 & 2 & 0 \\ 1 & -8 & 20 & -8 & 1 \\ 0 & 2 & -8 & 2 & 0 \\ 0 & 0 & 1 & 0 & 0 \end{bmatrix}$$

Correspondingly, the updating equation of the modified standard regularisation for V_{ij} is

$$V_{i,j}^{(t+1)} = V_{i,j}^{(t)} - 2\mu \left[(V_{i,j}^{(t)} - d_{i,j}) \right]$$

$$+ \lambda_1 \sum_{k=-1}^1 \sum_{l=-1}^1 S_2(k+1, l+1)V_{i+k, j+l}^{(t)} + \lambda_2 \sum_{k=-2}^2 \sum_{l=-2}^2 T_2(k+2, l+2)V_{i+k, j+l}^{(t)} \Big]$$

3.2 Edge-preserving smoothing model

The need for edge-preserving smoothing was studied on artificial data (Figs. 2–4). Without smoothing, the threshold surface intersected the unsmoothed image surface in both foreground and background regions (Fig. 2b). This gives spurious background pixels in the foreground regions, and *vice versa*. Smoothing by using a standard regularisation on the other hand made narrow peaks and valleys in the ideal data weak in the smoothed image (Fig. 3a), and consequently they tend to disappear after binarisation (Fig. 3b). Therefore a smoothing method that preserves edge information was necessary.

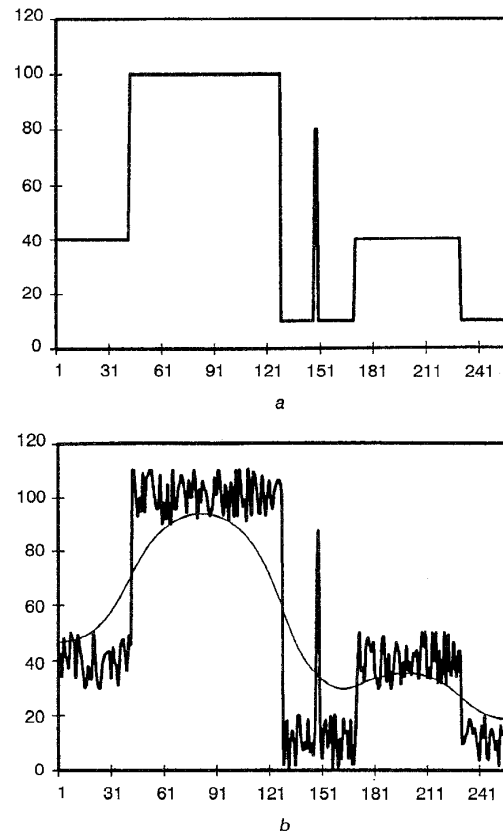


Fig.2 Showing need for using edge-preserving model, see also Figs. 3 and 4

a Ideal data
b Threshold surface intersected the image surface
— noisy data
— threshold surface

Based on the gradient descent method, we obtain the solution to the energy function of the edge-preserving smoothing model by using the following updating equation. The updating equation for the 1-D case is

$$V_i^{(t+1)} = V_i^{(t)} - 2\mu \left[(V_i^{(t)} - d_i) + \frac{1}{2}\lambda \left(g'_{Huber}(V_i^{(t)} - V_{i-1}^{(t)}) + g'_{Huber}(V_i^{(t)} - V_{i+1}^{(t)}) \right) \right]$$

for $i = 1, 2, \dots, N_x$

and the updating equation for the 2-D case is

$$V_{i,j}^{(t+1)} = V_{i,j}^{(t)} - 2\mu \left[(V_{i,j}^{(t)} - d_{i,j}) + \frac{1}{2}\lambda \left(g'_{Huber}(V_{i,j}^{(t)} - V_{i+1,j}^{(t)}) + g'_{Huber}(V_{i,j}^{(t)} - V_{i-1,j}^{(t)}) + g'_{Huber}(V_{i,j}^{(t)} - V_{i,j+1}^{(t)}) + g'_{Huber}(V_{i,j}^{(t)} - V_{i,j-1}^{(t)}) \right) \right]$$

where

$$g'_{Huber}(\xi) = \begin{cases} 2\xi, & |\xi| \leq \gamma \\ 2\gamma, & \xi > \gamma \\ -2\gamma, & \xi < -\gamma \end{cases}$$

By using edge-preserving smoothing, narrow peaks and valleys were preserved, and at the same time enough noise was removed to avoid spurious mislabelled pixels (Figs. 4a and b).

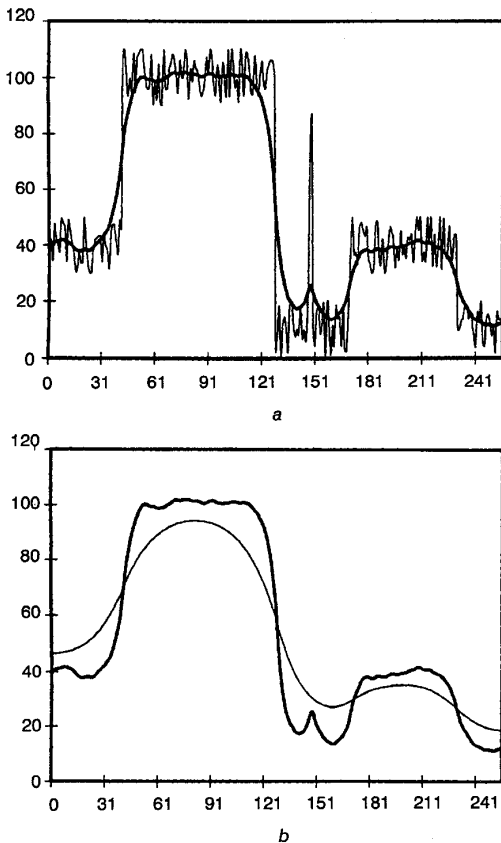


Fig. 3 Showing need for using edge-preserving smoothing model, see also Fig. 4
a Narrow peak becoming weak after standard smoothing
 — noisy data
 — smoothed data
b Peak lost after binarisation
 — threshold data
 — smoothed data

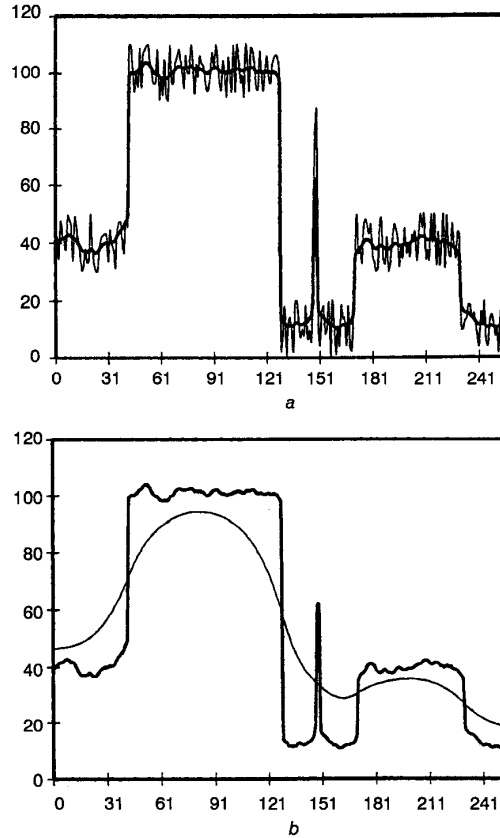


Fig. 4 Showing need for edge-preserving smoothing model
a Peak retained after edge-preserving smoothing model
 — noisy data
 — smoothed data
b Peak still present after binarisation
 — threshold data
 — smoothed data

4 Experimental results

Fig. 5 shows 1-D data, where the noisy data in Fig. 5b is the corrupted version of the ideal one in Fig. 5a. The smoothed data in Fig. 5b is obtained by using our edge-preserving smoothing model with parameters $\mu = 0.005$ (learning rate), $\gamma = 2.0$ and $\lambda = 70.0$. The threshold surface in Fig. 5c is obtained by our modified standard regularisation with parameters $\mu = 0.005$ (learning rate), $\lambda_1 = 200.0$ and $\lambda_2 = 10.0$.

Four 2-D test examples are shown in the top row of Fig. 6, (a1–d1). These images are all of size 256×256 pixels, and all of them are nonuniformly illuminated images corrupted by random noise. Figs. 6a1 and b1 are artificially generated, and Figs. 6c1 and d1 are real images. The original version of Fig. 6d1 was captured by a scanner and gaussian noise added to become Fig. 6d1. For Fig. 6a2, edges can be detected by the Canny edge detector, Fig. 7a4, however, for Figs. 6b2, c2, d2, some false edges appear owing to noise and some object edges disappear owing to low contrast (Figs. 7b4, c4, d4).

Figs. 6a2, b2, c2, d2 are the respective smoothed versions of Figs. 6a1, b1, c1, d1 after using our edge-preserving smoothing model. For comparison, all of the four adaptive methods (our method, SORM, and Parker's method and Niblack's method) are performed on the same smoothed image. Notice the postprocessing step from Yanowitz and Bruckstein's method is not

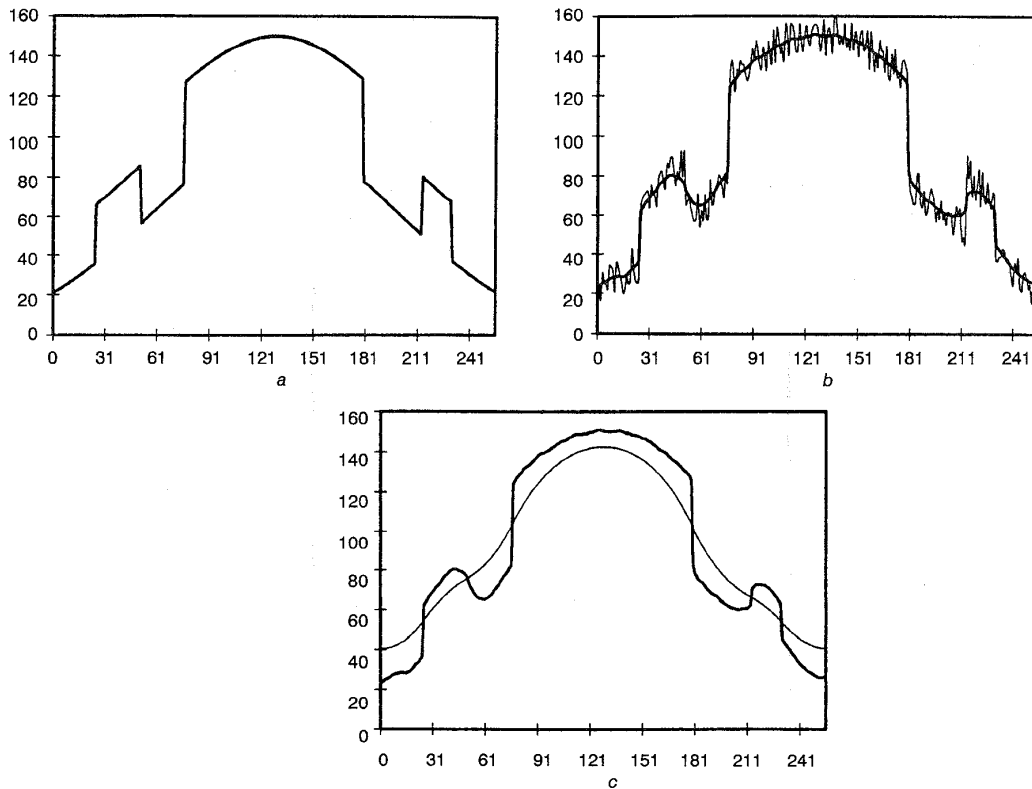


Fig.5 Experiment on 1-D nonuniform and noisy data by our method

a Ideal data
 b Noisy data and smoothed version
 — noisy data
 — smoothed data
 c Smoothed data and threshold surface
 — threshold surface
 — smoothed data

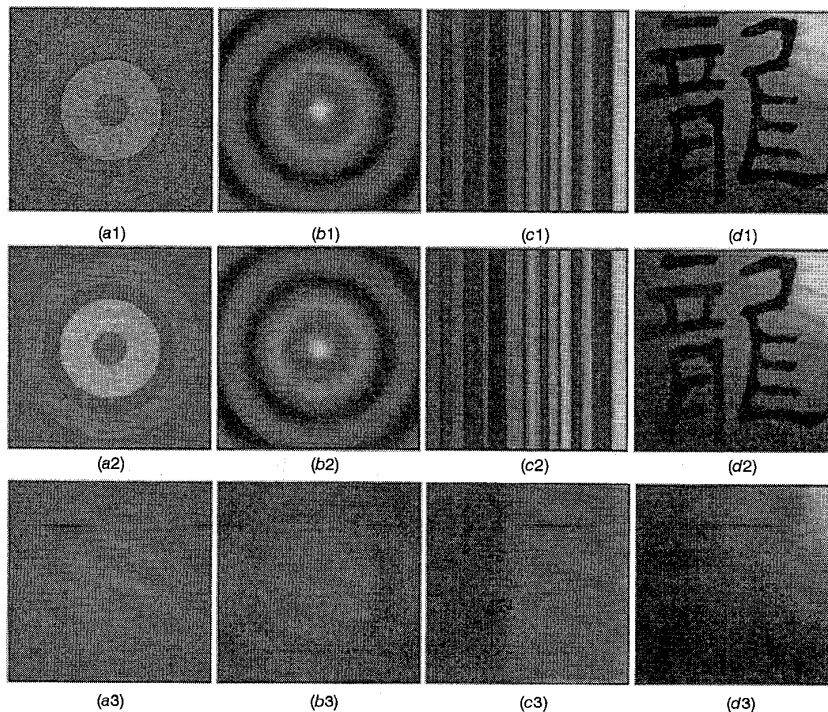


Fig.6 Experiment on 2-D images: comparison of four methods (our method, SORM, Parker's method, Niblack's method) (see also Fig. 7)

a1-d1 Four test images
 a2-d2 Images smoothed by edge-preserving smoothing model
 a3-d3 Threshold surfaces calculated by our modified standard regularisation

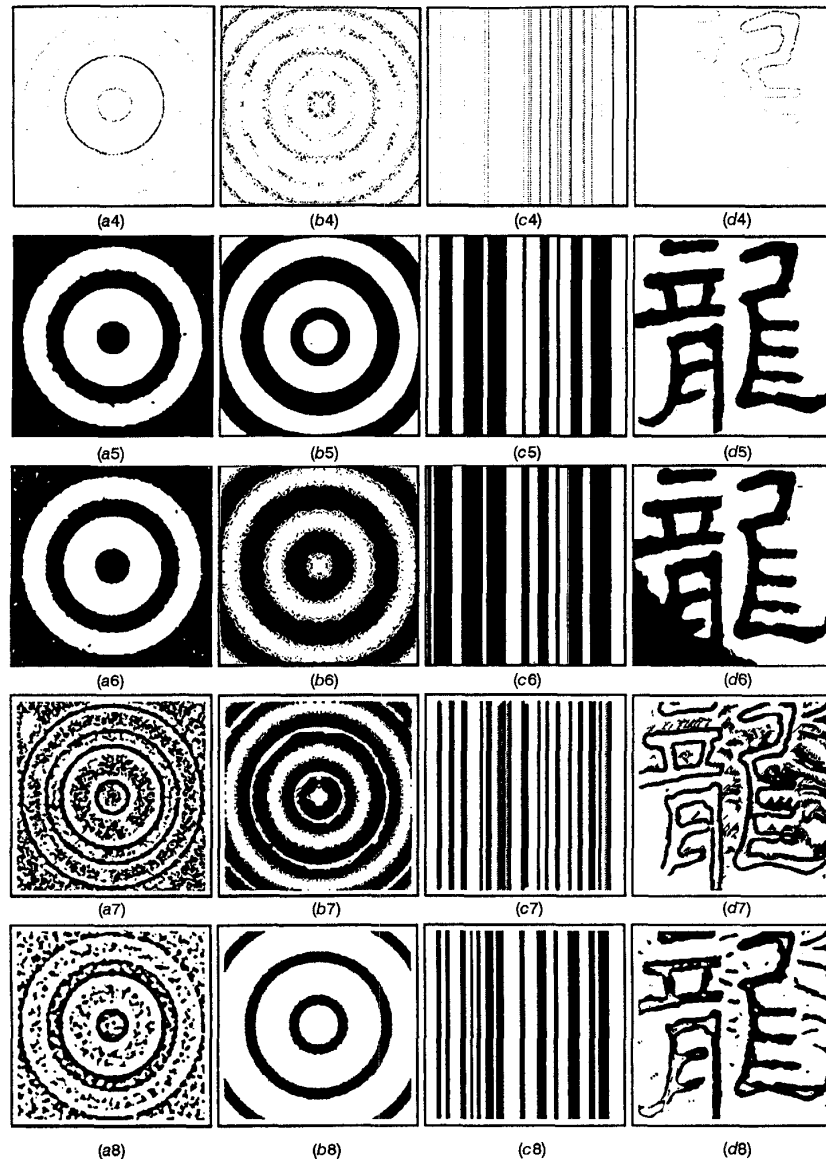


Fig. 7 Experiment on 2-D images: comparison of performance of four methods (ours, SORM, Parker's and Niblack's)
a4-d4 Edge maps by Canny edge detector
a5-d5 binarisation results by our method
a6-d6 SORM
a7-d7 Parker's method
a8-d8 Niblack's method

applied in all four methods, including Parker's and Niblack's methods. Figs. 6a3, b3, c3, d3 are the threshold surfaces obtained by our modified standard regularisation, respectively, for Figs. 6a2, b2, c2, d2.

Using these threshold surfaces, our method obtained good binarisation results as shown in Figs. 7a5, b5, c5, d5. Since SORM is based on edge information to interpolate the threshold surface, the performance of SORM is affected by the correctness of edge detection. Figs. 7a4, b4, c4, d4 show the corresponding Canny-edge maps of the smoothed images given in Figs. 6a2, b2, c2, d2. The binarisation results generated by SORM are shown in Figs. 7a6, b6, c6, d6. Since the object edges in Fig. 7a4 are stronger than the false edges, the binarisation result by SORM in Fig. 7a6 is acceptable. However, the binarisation results by SORM in

Figs. 7b6, c6, d6 are not so good since false edges appear in the edge maps of Figs. 6b4, c4 and object edges were lost in the edge map of Fig. 6d4. Figs. 7a7, b7, c7, d7 show the binarisation results by Parker's methods, while Figs. 7a8, b8, c8, d8 give the results by Niblack's method. From all these experimental results, it is easy to conclude that our method offers the best binarisation performance over the other three methods.

For our method the parameters for edge-preserving smoothing on 2-D images are $\mu = 0.0035$ (learning rate), $\gamma = 0.5$ and $\gamma = 120.0$. The parameters for the modified standard regularisation are $\mu = 0.0035$ (learning rate), $\lambda_1 = 400.0$ and $\lambda_2 = 40.0$. In SORM, $\beta = 1.0$ was chosen. In Niblack's method, the neighbourhood size 7×7 and $k = -0.2$ were used. In Parker's method, the region size 7×7 and parameters $m_0 = -1.0$, $s_0 = 1.0$

and $k = -1.0$ were chosen. The choices of parameters are based on our experience and the results given in [17].

Table 1: Processing time for four methods in seconds

	Fig.6(a1)	Fig.6(b1)	Fig.6(c1)	Fig.6(d1)
Our method	605	1460	190	954
SORM	3600	10658	1249	7632
Parker's method	29	10	18	12
Niblack's method	4	6	3	4

Processing times for the four methods are listed in Table 1, where the time is in seconds. Niblack's method is the fastest one among the four methods and Parker's method came second. However, the results generated are much worse than those obtained using our method and SORM's. Basically, our method gave better performance than SORM on binarisation results and in processing speed. Our method is about seven times faster than SORM.

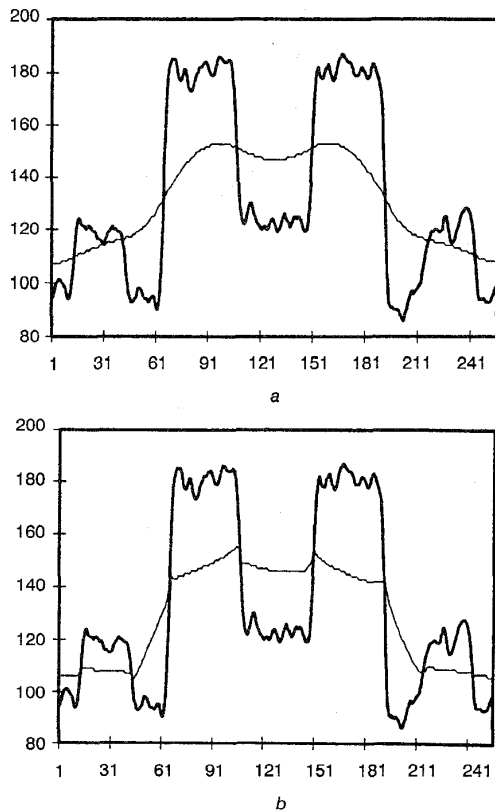


Fig. 8 Comparisons of threshold surfaces obtained by our method and SORM: 128th-row scan line of smoothed image of Fig. 6a2
a a1
 — 128th horizontal line
 — our threshold
b a2
 — 128th horizontal line
 — SORM's threshold

5 Discussion and conclusion

SORM depends on the edge segments to interpolate the threshold surface, which makes the interpolated threshold surface discontinuous and even incorrect, particularly when part of the edge segments were missed by the edge detector. Some object edges are lost owing to

low contrast (Fig. 7d4) and some false edges appear owing to noise (Figs. 7b4, c4), which affects the binarisation results. Figs. 8–11 compare the threshold surfaces obtained by our method and SORM. Three types of coarse curve in Figs. 8–10 are, respectively, the 128th-row scan lines of the smoothed images in Figs. 6a2, b2, and c2, while the coarse curve in Fig. 11 is the 70th-row scan line of the smoothed image in Fig. 6d2. All the four fine curves in Figs. 8–11a1, b1, c1, d1 are the threshold surfaces obtained by our method, and the other four fine curves in Figs. 8–11a2, b2, c2, d2 are the threshold surfaces by SORM. It can be seen from these curves that the threshold surfaces generated by our method are smoother and more reasonable. The reasons for making the SORM's threshold surfaces discontinuous are (i) object edges are not correctly extracted, and (ii) the threshold values on the edge positions are locked during the process of the interpolation.

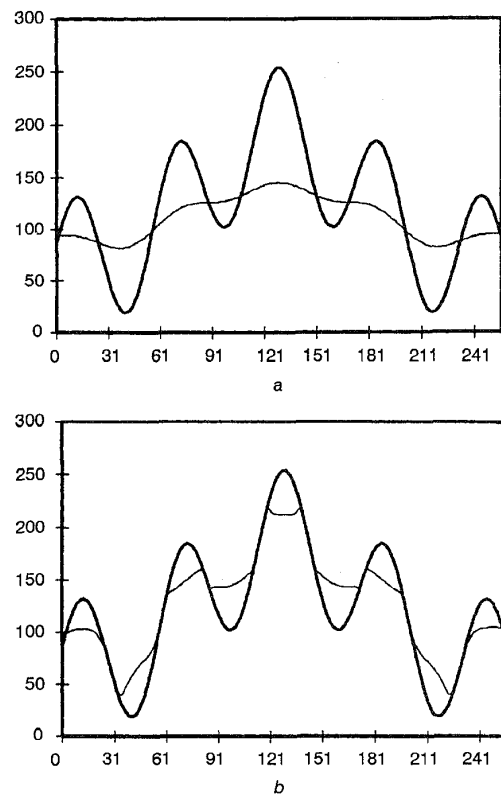


Fig. 9 Comparison of threshold surfaces obtained by our method and SORM: 128th-row scan line of smoothed image of Fig. 6b2
a b1
 — 128th horizontal line
 — our threshold
b b2
 — 128th horizontal line
 — SORM threshold

The smoothness requirement in the edge-preserving smoothing model, used as the preprocessing step in our method, usually removes useful detail. For example, Fig. 12a is an image with some noise. After edge-preserving smoothing, the image becomes blurred (Fig. 12b) and details such as hair are missed in the binarisation result (Fig. 12c).

In summary, we have presented a modified standard regularisation approach with an edge-preserving

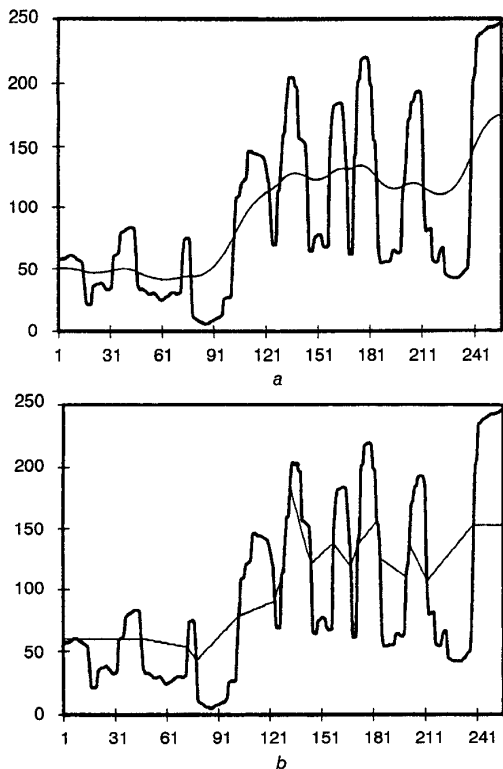


Fig. 10 Comparison of threshold surfaces obtained by our method and SORM: 128th-row scan line of smoothed image of Fig. 6c2
 a c1 ——— 128th horizontal line ——— our threshold
 b c2 ——— 128th horizontal line ——— SORM threshold

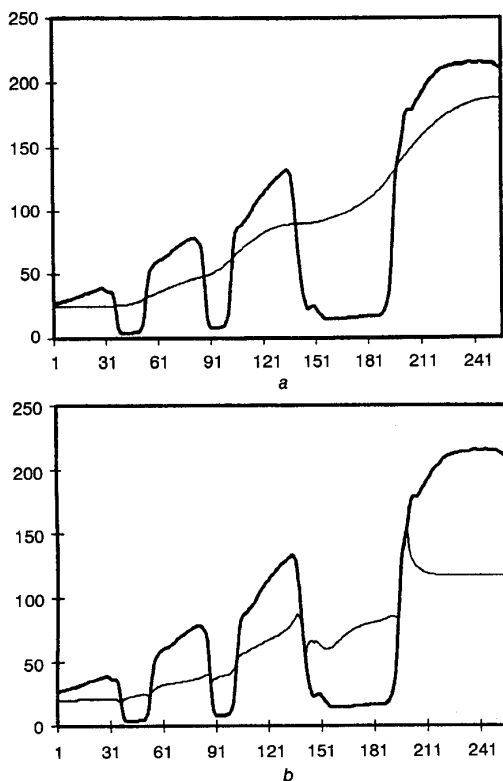


Fig. 11 Comparison of threshold surfaces obtained by our method and SORM: 70th-row scan line of smoothed image of Fig. 6d2
 a d1 ——— 70th horizontal line ——— our threshold
 b d2 ——— 70th horizontal line ——— SORM threshold

smoothing model as a preprocessing step for segmenting nonuniform and corrupted images. Since our method is independent on edge information and furthermore the energy functional of the modified standard regularisation has been reformulated by adding another penalty term $(Lap_2(i))^2$, our method gives better segmentation performance over SORM, Parker's method and Niblack's method, and is about seven times faster than SORM. Furthermore, similar to the technique described in [16], our method can be implemented efficiently using a Hopfield neural network.

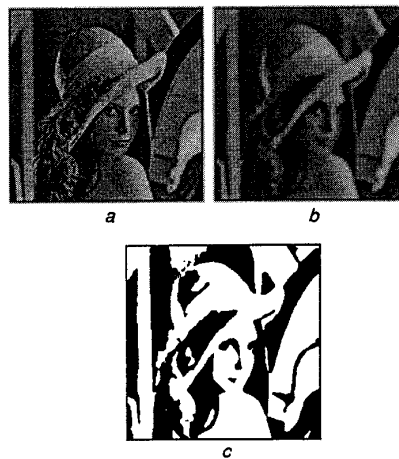


Fig. 12 Example of image which our method is unable to segment correctly owing to presmoothing
 a Noisy image
 b Smoothed image
 c Binarisation result

6 References

- GEMAN, S., and GEMAN, D.: 'Stochastic relaxation, Gibbs distributions, and the Bayesian restoration of images', *IEEE Trans.*, November 1984, **PAMI-6**, pp. 721-741
- DERIN, H., ELLIOT, H., CRISTI, R., and GEMAN, D.: 'Bayes smoothing algorithms for segmentation of binary images modeled by Markov random fields', *IEEE Trans.*, November 1984, **PAMI-6**, pp. 707-720
- DERIN, H., and ELLIOT, H.: 'Modeling and segmentation of noisy and textured images using Gibbs random fields', *IEEE Trans.*, January 1987, **PAMI-9**, pp. 39-55
- YAOU, M.H., and CHANG, W.T.: 'Fast surface interpolation using multiresolution wavelet transform', *IEEE Trans.*, July 1994, **PAMI-16**, pp. 673-688
- SZELISKI, R.: 'Fast surface interpolation using hierarchical basis functions', *IEEE Trans.*, June 1990, **PAMI-12**, pp. 513-528
- GEIGER, D., and GIROSI, F.: 'Parallel and deterministic algorithms from MRF's: surface reconstruction', *IEEE Trans.*, May 1991, **PAMI-13**, pp. 401-412
- SHULMAN, D., and HERVE, J.Y.: 'Regularization of discontinuous flow fields'. Proceedings of workshop on *Visual motion*, 1989, pp. 81-86
- STEVENSON, R.L., SCHMITZ, B.E., and DELP, E.J.: 'Discontinuity preserving regularization of inverse visual problem', *IEEE Trans.*, March 1994, **PAMI-24**, pp. 455-469
- BOUMAN, C., and SAUER, K.: 'A generalized Gaussian image model to edge-preserving MAP estimation', *IEEE Trans. Image Process.*, July 1993, **2**, (3), pp. 296-310
- LI, S.Z.: 'On discontinuity-adaptive smoothness priors in computer vision', *IEEE Trans.*, June 1995, **PAMI-17**, pp. 576-586
- SAHOO, P.K., SOLTANI, S., and WONG, A.K.C.: 'A survey of thresholding techniques'. *CVGIP*, 1988, Vol. 41, pp. 233-260
- PANDA, D.P., and ROSENFELD, A.: 'Image segmentation by pixel classification in (gray level, edge value) space', *IEEE Trans.*, 1978, **C-27**, pp. 875-879
- CHOW, C.K., and KANEKO, T.: 'Automatic boundary detection of the left-ventricle from cineangiograms', *Comput. Biomed. Res.*, 1972, **5**, pp. 388-410

- 14 NAKAGAWA, Y., and ROSENFELD, A.: 'Some experiments on variable thresholding', *Pattern Recognit.*, 1979, **11**, (3), pp. 191-204
- 15 YANOWITZ, S.D., and BRUCKSTEIN, A.M.: 'A new method for image segmentation', *CVGIP*, 1989, Vol. 46, pp. 82-95
- 16 SHEN, D., and IP, H.H.S.: 'A Hopfield neural network for adaptive image segmentation: an active surface paradigm', *Pattern Recognit. Lett.*, 1997, **18**, pp. 37-48
- 17 TRIER, Ø.D., and JAIN, A.K.: 'Goal-directed evaluation of binarization methods', *IEEE Trans.*, 1995, **PAMI-17**, (12), pp. 1191-1201
- 18 TIKHONOV, A.N., and ARSENIN, V.A.: 'Solutions of ill-posed problems' (Winston & Sons, Washington, 1977)
- 19 LI, S.Z., and HUANG, Y.: 'Edge-preserving smoothing by convex minimisation: closed-form solution and parameter selection'. Presented at ACCV'98, Jan. 1998